# 國立交通大學

顯示科技研究所

碩士論文

# 利用熱儲存層與細微結構增進側向結晶的研究與模擬

# Study of Simulation on Lateral Grain Growth Enhanced by Capping Layer and Microstructure


研 究 生：江俊德 Chun-Te Chiang

指導教授：李柏璁 教授 Prof. Po-Tsung Lee


中華民國九十七年七月

# Abstract (in Chinese)

本文主要模擬KrF(248nm)laser施打在a-Si膜表面後，因熱傳所造成的溫度分佈。並定義出潛熱作用時間爲結晶時間，在不考慮成核點的影響下，潛熱作用時間越長，結晶成長時間就越長。藉由比較結晶時間來討論加上熱儲存層$SiO_2$與$SiN_x$的優缺點，與增加環境溫度所造成的效應。其中隨著環境溫度的增加，在a-Si蓋上$SiO_2$有最佳值100nm造成最佳結晶時間，此外蓋上$SiN_x$隨著厚度增加，可以得到較長的結晶時間，在較低製程溫度可以得到較長結晶時間。最後引進溝渠定位長晶，模擬其熱流分布，找到其溝渠最小間隔，與最佳溝渠深度，藉由紀錄其固液接面，算出其結晶速度，並估計其結晶大小。

# Abstract (in English)

In this thesis we simulate the heat transfer inside the a-Si thin film after KrF laser annealing. And by defining latent heat process region, the temperature distribution among the samples can be successfully measured. Not concerning nucleation effect, the recrystallization time becomes longer with the solidifying duration. We find that the thickness of $SiO_2$ capping layer has an optimized value 100nm with and without trench, and that of SiNx capping layer thicker than 100nm has better performance on solidifying duration compared with the same thickness of $SiO_2$ capping layer. We simulated the trench-assisted ELA. And we find out its optimized trench depth, 300nm, and its smallest separation, 2 $\mu$m. It is proved that trench-assisted position-control ELA can induce lateral grain growth by observing the isothermal diagram. By recording the movement of the 1350K isothermals, we can calculate the isothermal moving velocity, namely solid-liquid interface velocity. Finally, we can estimate the grain size from a trench to one side is about 3 $\mu$m for an optimized condition. In a word, utilizing a trench can induce about 6 $\mu$m lateral grain growth.

## Acknowledgements (致謝)

在這短短的碩士生日子當中，首先要感謝我的家人，外公外婆，父母，及2個弟弟。沒有你們的大力支持，就沒有今天的我。我是個任性又固執的傢伙，感謝你們的包容，讓我無後顧之憂的求學，我想要把這個功勞獻給你們。

首先要感謝我的老師，李柏璁老師，謝謝你提供我一個超自由的學習環境，感謝您這幾年的大力指導，讓我獲益匪淺。在我實驗遇到困難時，並沒有急言厲色的斥責我，反而給我機會讓我去摸索，尤其最後一關拉我一把，費心幫我理出邏輯，潤飾投影片，修改論文。此外謝謝冉曉雯老師，雖然我蠻怕你的，但是的你建議都是非常直接而且有見地的，也是你領我進入半導體與TFT的領域，在此非常感謝你。

再來要謝謝本實驗室的台柱，謝謝贊文，你讓我看到博士班的專精；謝謝資岳，你讓我看到博士班的涉獵領域的廣度；謝謝明峯學長，你讓我看到博班的熱情。

我是個幸運的人，讓我在的碩一遇到不錯的學長，阿蘇，書志，鴻祺，峻豪，阿懋學長，當然還有元老的強哥，竑鈞，你們面對事情的積極態度，一起插科打渾，一起出遊，讓我在碩一過得很快樂，都深深的影響我。感謝阿蘇毫不保留與耐心的教我實驗步驟，也要謝謝跟我同屆的思元，嘉銘，仲銓，佳禾，讓我碩士修課，考試，做實驗都有個伴，尤其要感謝佳禾和嘉銘在趕畢業之際，特別抽出時間幫我趕實驗時，大力幫我寫E-Beam，點滴在心頭。感謝耿睿，書豪，士民，俊銘，耀慶，陪我運動，鍛鍊我的意志；劉維仁學長，楊松學長，黃同慶學長給我材料分析方面的意見；啓銘，唐豪，逸立，振欽，振銘，志剛學長，與我討論製程上面的問題。

謝謝學弟和璁辛苦的幫我打雷射，我真的欠你很多，均融，孟穎，在我需要試片幫我寫EBEAM，宜育幫我做ICP，明璽懷我見識到PTT的世界，幫我帶來歡樂。怡先帶我運動，韋德，欣育，逸華，青樺，香君幫我加油打氣。

感謝阿蘇，書志，鴻祺，甚至在畢業之後，在我實驗困頓時，仍不時打電話鼓勵我。資岳學長，幫我找尋機台。明峯學長在我最後一年，陪我熬夜做實驗，一起討論，你帶給我許多正面的想法。也謝謝曾經有2位學長在我實驗困頓之際，願意提供數據與想法幫我畢業，雖然我婉拒了，但是你們的友情相挺，卻重新燃起我的鬥志讓我無後顧之憂，繼續往前衝。

我是一個幸運的人。在我進入研究所我立下的願望是改變自己。雖然一開始我想學光學，後來接觸製程，最後以熱流模擬畢業，也曾經認爲做熱流模擬爲什麼當初不回機械所做研究，但是上天其實看的比我透徹，他是藉由這個機會，訓練我，點出我的弱點，給我機會補足我不足的地方，讓我由意志不堅定的小伙子，懂得去探索自己的極限，堅持下去，讓我完成改變自己的初衷。

謝謝你們幫我自我探索，敲開一塊牆，讓我踏出第一步，如今我將遠行，但是害怕我會健忘，忘了在此養成的習慣與經驗，所以誌文表達感謝之意，與警惕自己時時銘記在心---我還沒有成功，這只是個開始。

2008于新竹交大

江俊德

# Index

*Abstract (in Chinese)* ........ i

*Abstract (in English)* ........ ii

*Acknowledgements (致謝)* ........ iii

*Index* ........ v

*Figure List* ........ vii

*Table List* ........ ix

**CHAPTER 1. INTRODUCTION ........ 1**

1.1. OVERVIEW OF ACTIVE MATRIX LIQUID CRYSTAL (AMLCD) ........ 1

1.2. THE PURPOSE OF LASER ANNEALING (LA) ........ 3

1.3. POSITION CONTROL GRAIN GROWTH ........ 7

1.4. THE THEORY OF CRYSTALLIZATION ........ 8

1.5. MOTIVATION ........ 12

**CHAPTER 2. SIMULATION ........ 13**

2.1. HEAT TRANSFER EQUATION ........ 13

2.2. HEAT FLUX SIMULATION ........ 14

2.3. SIMULATION CONDITION WITH $SIO_2$ CAPPING LAYER ........ 20

2.4. SIMULATION CONDITION WITH $SIN_X$ CAPPING LAYER ........ 22

**CHAPTER 3. SIMULATION WITH TRENCH-ASSISTED POSITION CONTROL ........ 25**

3.1. FIND OUT THE SMALLEST SEPARATION BETWEEN THE TRENCHES AND OPTIMIZED TRENCH DEPTH 25

3.2. SIMULATION TRENCH-ASSISTED POSITION CONTROL WITH $SIO_2$ CAPPING LAYER ........ 28

3.3. CALCULATION OF SOLID-LIQUID INTERFACE AND ESTIMATION OF GRAIN SIZE ........ 30

**CHAPTER 4. SUMMARY AND FUTURE WORK ........ 34**

4.1. SUMMARY........................................................................................................................ 34

4.2. FUTURE WORK ................................................................................................................... 35

**REFERENCE ................................................................................................................................ 36**

# Figure List

FIGURE 1-1 METHODS FOR MANUFACTURE POLY-SI THIN FILM. .... 3

FIGURE 1-2 AVERAGE GRAIN SIZE VS LASER INTENSITY PLOT .... 5

FIGURE 1-3 TIME DEPENDENCE OF SI-LAYER MELT FRONT PROFILES UNDER EXCIMER LASER IRRADIATION . 5

FIGURE 1-4 SAMPLE STRUCTURE WITH CAPPING LAYER DEPOSITED ON A-SI. .... 6

FIGURE 1-5 (A) THE FABRICATION PROCESS OF THE GRAIN FILTER, (B) AND (C) MATRIX-ARRAY GRAINS BY THE GRAIN FILTER METHOD, (D) THE CRYSTALLIZATION PROCESS IN A GRAIN FILTER. .... 8

FIGURE 1-6 SHOW TWO PHASES AND THE PHASE TRANSFORMATION REGION THAT LATENT HEAT OCCUR ..... 9

FIGURE 1-7 TEMPERATURE CURVE OF THE OUTPUT SIGNAL OF THE PYROMETER SENSOR. .... 10

FIGURE 1-8 TEMPERATURE CURVE OF A PARTICULAR POINT VERSUS THE TIME .... 11

FIGURE 2-1 THE LEFT PART OF PICTURE IS THE NORMAL MESHES IN THE STRUCTURE AND THE RIGHT PART IS THE REFINED MESHES IN THE STRUCTURE. THE REFINE MESHES WOULD INCREASE THE ACCURACY OF THE FINAL RESULT. .... 14

FIGURE 2-2 THE STRUCTURE FOR A SIMPLE SIMULATION, THE TOP LAYER IS -SI AND THE BOTTOM LAYER IS $SIO_2$. THE DIMENSIONS AND THE BOUNDARY CONDITIONS OF EACH SIDE ARE LABELED ON IT. .... 16

FIGURE 2-3 (A) THERMAL DISTRIBUTION AT A CERTAIN TIME = 800 NS, (B) THE CONTOUR LINES OF THE TEMPERATURE AND THE HEAT FLUX AT A CERTAIN TIME = 800NS (C) TEMPERATURE CURVE OF A PARTICULAR POINT (1.5 M, 1.1 M) VERSUS THE TIME (D) TEMPERATURE CURVE OF A PARTICULAR LINE (ALONG THE RED LINE IN FIGURE 2.2) VERSUS THE TIME (AT 25NS, 55NS, 85NS AND 115NS) ..... 18

FIGURE 2-4 (A) TEMPERATURE CURVE OF A PARTICULAR POINT VERSUS THE TIME (B) ISOTHERMAL MOVEMENT DIAGRAM IN SOLIDIFYING DURATION. .... 19

FIGURE 2-5 THE SIMPLE STRUCTURE WITH SIO2 CAPPING LAYER .... 20

FIGURE 2-6 THE PROCESS FLOW OF HEAT TRANSFER AFTER LASER IRRADIATION WITH CAPPING LAYER $SIO_2$ .... 20

FIGURE 2-7 THE SOLIDIFYING DURATION DIAGRAM WITH DIFFERENT $SIO_2$ THICKNESS AND DIFFERENT

AMBIENT TEMPERATURE ........................................................................................................... 21

FIGURE 2-8THE SIMPLE STRUCTURE WITH $SIN_X$ CAPPING LAYER ........................................................... 22

FIGURE 2-9 THE PROCESS FLOW OF HEAT TRANSFER AFTER LASER IRRADIATION WITH CAPPING LAYER $SIN_X$ ........................................................................................................................................ 22

FIGURE 2-10 THE SOLIDIFYING DURATION DIAGRAM WITH DIFFERENT $SIO_2$ THICKNESS ............................ 23

FIGURE 3-1 (A) STRUCTURE OF EACH TRENCH (B) THE STRUCTURE OF TWO TRENCHES ............................ 25

FIGURE 3-2 (A)TEMPERATURE CURVE ON THE A-SI SURFACE WITH 1MM SEPARATION TRENCH (B) TEMPERATURE CURVE ON THE A-SI SURFACE WITH 2MM SEPARATION TRENCH ................................ 26

FIGURE 3-3 THE STRUCTURE FOR FINDING OPTIMIZED TRENCH DEPTH ....................................................... 27

FIGURE 3-4THE STRUCTURE FOR FINDING OPTIMIZED THICKNESS OF SIO2 CL ........................................... 28

FIGURE 3-5 THE SOLIDIFYING DURATION DIAGRAM WITH DIFFERENT $SIO_2$ THICKNESS .............................. 29

FIGURE 3-6 THE ISOTHERMAL MOVEMENT DIAGRAM IN SOLIDIFYING DURATION. ....................................... 30

FIGURE 3-7 S-L INTERFACE VELOCITY DIAGRAM AT AMBIENT TEMPERATURE 27℃ WITH DIFFERENT THICKNESS OF $SIO_2$ CAPPING LAYER ........................................................................................................ 31

FIGURE 3-8 (A) SOLIDIFYING DURATION DIAGRAM, (B) S-L INTERFACE VELOCITY DIAGRAM AND (C)THE ESTIMATION GRAIN SIZE DIAGRAM AT AMBIENT TEMPERATURE 27℃ .............................................. 31

FIGURE 3-9 1350-ISOTHERMAL MOVEMENT AT TA=27℃ WITH TRENCH 300NM DEPTH AND NO CAPPING LAYER ........................................................................................................................................ 33

# Table List

TABLE 1-1 DIFFERENT EXCIMER LASER GASES AND CORRESPONDING WAVELENGTHS ................................ 4

TABLE 1-2 STEADY-STATE SOLIDIFICATION (POSITIVE) AND MELTING (NEGATIVE) VELOCITIES AS DETERMINED AT EACH TEMPERATURE USING MOLECULAR-DYNAMICS SIMULATION. ........................ 11

TABLE 2-1 THERMAL CONDUCTIVITY, SPECIFIC HEAT AND OTHER PARAMETERS USED IN THE SIMULATION. THE VALUE OF ABSORPTION COEFFICIENT WAS MEASURED BY N&K ANALYZER. .............................. 17

TABLE 3-1 THE SOLIDIFYING DURATION ON THE A-SI SURFACE 2   M AWAY FROM THE TRENCH WITH DIFFERENT TRENCH DEPTH AND LASER ENERGY DENSITY. ................................................................ 27

# Chapter 1. Introduction

## 1.1. Overview of Active Matrix Liquid crystal (AMLCD)

Since 1961 P. K. Weimer firstly conceived the idea of thin-film transistors (TFTs) [1], Brody et al. built the first active matrix liquid crystal display (AMLCD) with switching elements, TFTs [2]. Not until Spear and LeComber constructed the first amorphous silicon (a-Si) TFTs in 1979 [3], the TFT-LCD industry had energized the following studies and investigations on a-Si TFTs. There are many kinds of active devices used for a backplane of AMLCD; they are amorphous silicon (a-Si) TFTs, high temperature poly-Si (HTPS) TFTs, low temperature poly-Si (LTPS) TFTs, and organic semiconductor TFT, which is under development. The main stream in TFT industry is to utilize a-Si TFTs and poly-TFTs technology for mass production nowadays. The a-Si TFTs can be fabricated on very large substrates at a very low cost with uniform TFT characteristics. However, the mobility of the a-Si TFTs is only about 1cm2/V/Sec. The mobility is too low to integrate the peripheral ICs, such as central processing units (CPUs), digital signal processors (DSPs), and memories etc. In a word, this disadvantage constraints the development of system on glass (SoG) or system on panel (SoP). Comparing to the a-Si TFTs, the poly-Si TFTs has higher carrier mobility up to 200cm2/V/Sec. With higher mobility, the flat panel display (FPD) can reduce the device dimension, acquire higher aspect ratio, increase brightness, and reduce power consumption. In another view, higher mobility results in higher pixel driving TFT on-current, reduces RC delay time, and brings about large reduction in pixel charging duration. Moreover, the poly-Si TFTs have an opportunity to realize SoG.

Poly-Si can be produced in several ways. It can be classified into two groups, HTPS and LTPS, according to its process temperature [4]. One of the HTPS methods is to directly

deposit poly-Si film directly on the samples at high temperature (> 600℃) by LPCVD. The process is simple, and the TFTs can get higher mobility up to 200cm$^2$/V/Sec. The substrate demands for quartz(melting temperature ~ 1000℃) which can endure over 600 ℃. It increases the production cost and limits the development of large size TFT -LCD. The other method is to initially deposit an a-Si thin film and anneal in a furnace for a long time, called solid-phase-crystallization (SPC). Amorphous silicon is a thermodynamically metastable phase. When the a-Si film obtains a sufficient energy to overcome the initial energy barrier, the a-Si starts to transfer to poly-silicon. The SPC can be undergone with a wide temperature process window corresponding to annealing times. According to the micro-structural pictures of the precursor-Si film, the relation between annealing temperature and annealing time is not unique [5], because of the random nucleation rate. With different deposition method and conditions [6][7], the nucleation rate would be strongly influenced. By increasing the deposition rate and the decreasing the temperature, the silicon film will form a serious structural disorder that induces the silicon hard to nucleation. Metal Induced Lateral Crystallization (MILC) is an improvement method for SPC. It decreases the activation energy of Si and enhances the grain growth under the lower process temperature (500~550℃). However, it needs to spend about 10hr for grain growth and has an issue for metal residuum in the active layer of poly-Si TFT. In order to reduce the crystallization temperature -time and obtain higher mobility at the same time, laser-annealing is a potential technology to achieve such performance demands.

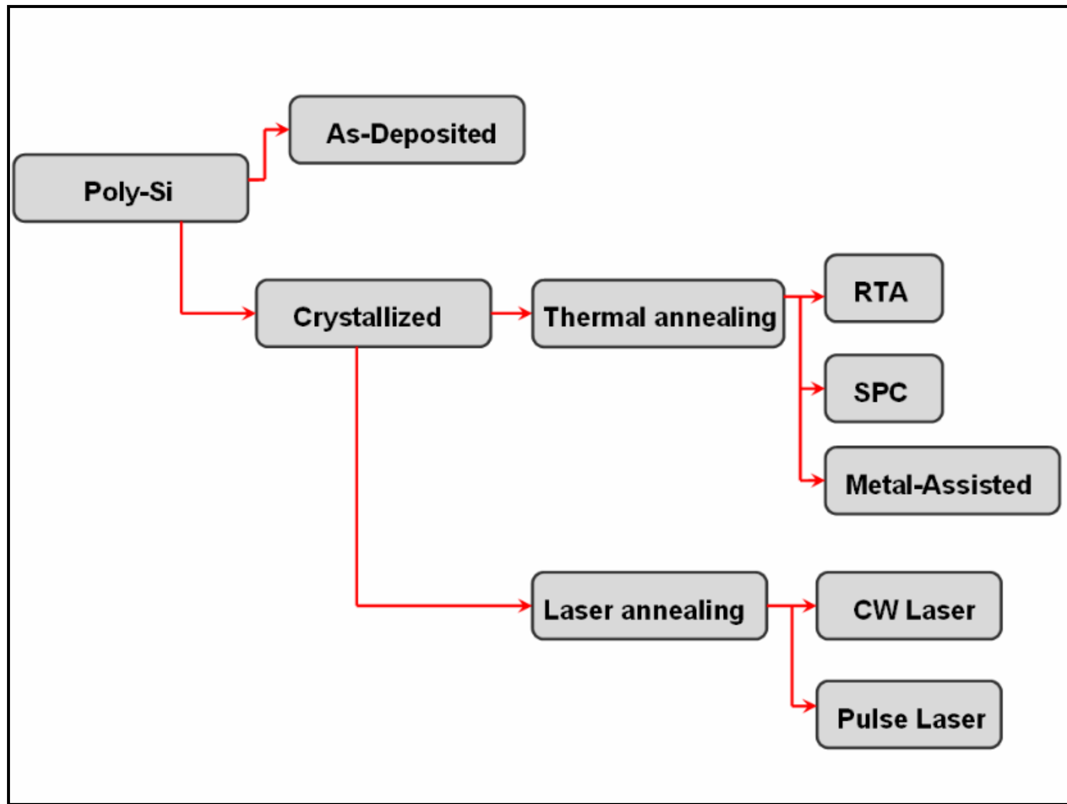


Figure 1-1 Methods for manufacture Poly-Si thin film.

## 1.2. The Purpose of Laser Annealing (LA)

The field of laser annealing and laser crystallization can be stemmed from the late 1970s. One of the exploitations of laser annealing is the removal of implantation damage and the subsequent electrical activation of dopants. Another application is to fabricate thin single-crystal semiconductors and alloys, such as Si, Ge, SiGe, or other high-K materials etc.

For poly-Si TFT manufacturing, the laser annealing technology is particularly important for advanced flat panel display utilization. Among the laser annealing technology, it can be departed into two parts, continual laser crystallization (CLC) and pulse-to-pulse laser annealing, due to pulse durations. This thesis focuses on pulse-to-pulse laser annealing, especially excimer laser annealing, which is widely used in TFT industry nowadays.

A major advantage of laser crystallization over conventional heating methods is its ability to limit rapid heating and cooling to thin surface layer. This is mainly controlled by the pulse duration time and the absorption depth of the laser light used in the material. A novel technology, excimer laser annealing (ELA), was introduced to enhance the crystallinity of the a-Si films in this study, and result in low thermal budget and small thermally induced stress. 錯誤! 找不到參照來源。 shows that the various wavelengths, between 157~351 nm, can be obtained using different laser gas, and all excimer lasers are pulsed laser modes.

| Laser gas | F2 | ArF | KrCl | KrF | XeCl | XeF |
|---|---|---|---|---|---|---|
| λ (nm) | 157 | 193 | 222 | 248 | 308 | 351 |

Table 1-1 Different Excimer laser gases and corresponding wavelengths

Fig. 1-2 shows that the average grain size is plotted as a function of the laser energy intensity. Samples prepared at room temperature and with low laser energy intensity were composed of small grains. With increasing laser energy density the average grain size increases and eventually reaches a maximum value. But when the energy density above maximum value, the grain size decreases to a constant value. According to the above, the optimal energy density is limited in a narrow region.

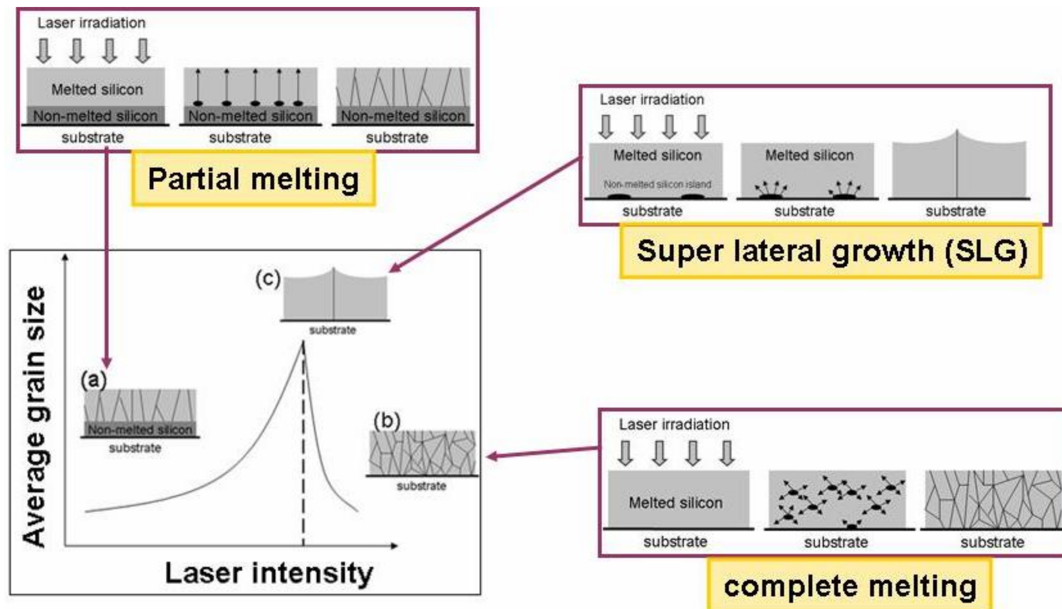


Figure 1-2 Average grain size vs laser intensity plot

Fig. 1-4 [8]shows the time dependence of Si-layer melt front profiles under excimer laser irradiation. It is assumed the whole Si layer was completely melted. As shown in this figure, the melting duration of the Si-layer is prolonged with increasing substrate temperature. The slope of the melt depth verses time graph decreases with increasing substrate temperature during excimer laser annealing.

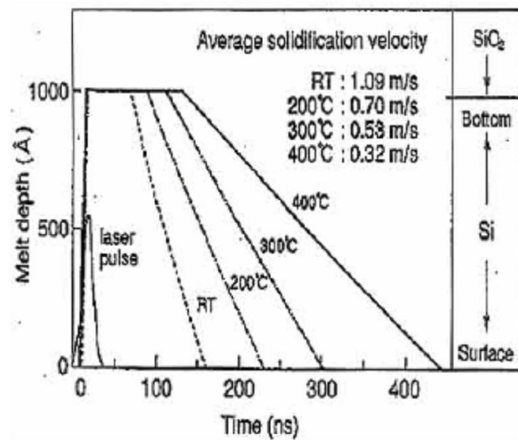


Figure 1-3 Time dependence of Si-layer melt front profiles under excimer laser irradiation

There are variable process parameters such as annealing ambient, laser duration, type of annealed films and substrate, which will affect the re-crystallized process. Besides, the physical parameters such as melting point, latent heat, thermal conductivity, density, specific heat, absorption coefficient, of annealed films must be serious considered first.

In order to widen the laser annealing process window, the capping layer (Figure 1 -3) is used to reduce heat loss from a-Si surface and feedback the heat when the a-Si undergoes the solidifying situation. Moreover, capping light-sensitive layer can absorb more laser intensity and results to feedback more heat to prolong solidifying situation. And then we got better grain growth.

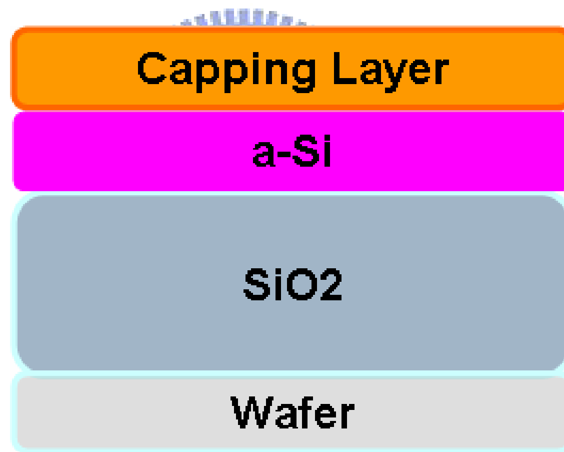


Figure 1-4 Sample structure with capping layer deposited on a-Si

## 1.3. Position control grain growth

There are two issues for manufacturing poly-Si TFT by conventional ELA. One is small process window, and the other is that random nucleation results in uncontrollable grain boundary, then the TFT electrical properties are not uniform over the whole flat panel. The grain location is controlled in 1D by the lateral growth of the molten Si. Several modulated excimer laser annealing methods have been proposed to realize large grains, such as sequential super lateral growth (SLG), selectively enlarging laser crystallization (SELAX)[9], continuous-wave (CW) laser lateral crystallization, phase-modulated excimer laser annealing (PMELA) [10], and so on. The grain size varies from 1 μm to 10 μm. To produce high performance TFTs, the channel is thus positioned parallel to the GBs, as shown in Figure 1.3(b). The field-effect electron mobility of TFTs approaches 400 cm2/Vs, and a rather high subthreshold swing is obtained due to the presence of GBs. However, the number of these parallel grain boundarys varys from device to device, leading to large variations in the characteristics.

We focus on changing structure to provide lateral grain growth. The $\mu$-Czochralski (Figure 1-5)basically uses locally increased thickness of the a-Si film and geometric selection of grains through a vertical narrow constriction. The positions of the grains can be controlled by local melting/unmelting of the Si film.

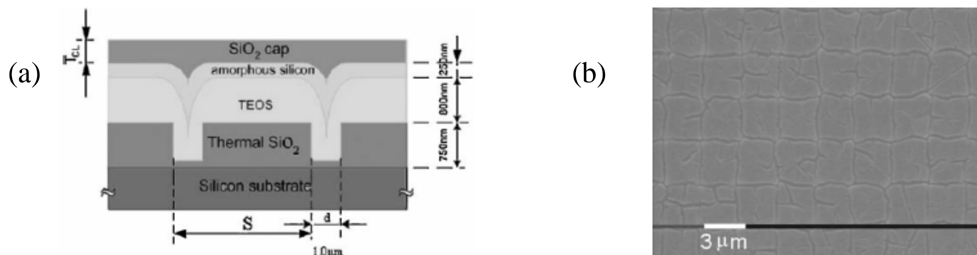

(c) 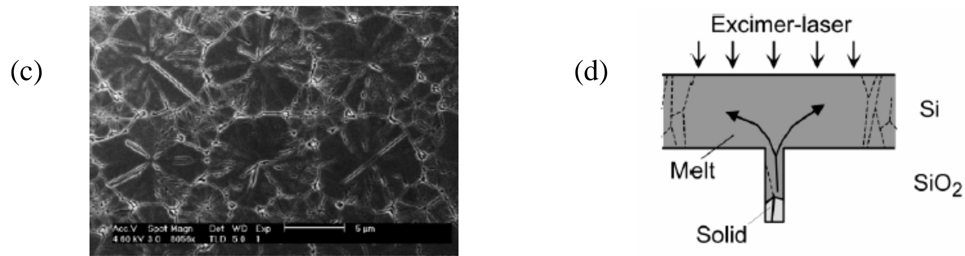 (d)



Figure 1-5 (a) the fabrication process of the grain filter, (b) and (c) matrix -array grains by the grain filter method, (d) the crystallization process in a grain filter.

## 1.4. The Theory of Crystallization

The fraction of laser light absorbed by the specimen creates electrons that thermalize with a time constant 10-11ns. In this very short time the electrons will approach a thermal equilibrium with the lattice, and thus transfer a part of the deposite d energy to phonons. Eventually, heat propagates through the simple by phonon and charge carrier diffusion. In order to acquire detailed knowledge of processes such as laser -induced implantation annealing and phase transformation it is essential to underst and the evolution of the temperature distribution in time and space. A significant contribution was the early development of a model to describe the phase transformation of ion-implanted silicon in terms of liquid-phase epitaxy due to pulsed laser irradiat ion. In this model, the standard heat equation was modified to include laser light absorption. Numerical solutions gave access to the time -dependence of the sample temperature as a function of laser intensity and pulse length.

Cerny and Prikryl et al. review the essential models developed to account for laser-induced phase changes in single crystal and amorphous silicon. The emphasis of their work resides in the latter material deposited on amorphous substrates such as glass and quartz. The model presented includes the phenomenon of exclusive crystallization [11], which taken into account that the polycrystalline, amorphous, and liquid phases

may exist and that phase changes occur between those phases (Figure 1-5).

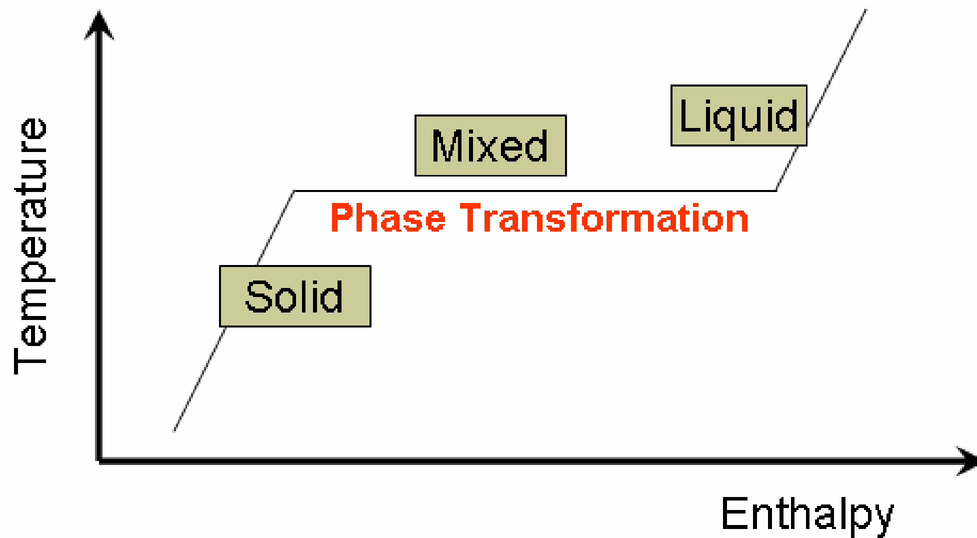


Figure 1-6 Show two phases and the phase transformation region that latent heat occur

Moreover, the model includes the time-dependence of the position of the liquid-vapor interface. All phase changes are considered non-equilibrium because of the speed of the crystallization process. Although some experimentally identified mechanisms are represented well in computational modeling, even advanced models cannot describe all experimental data. A good example is the phase-change process of a-Si where theory is still limited to homogeneous phase-change processes using the one-dimensional (1D) approximation and not taking into account nucleation effects. Furthermore, a mathematical model of non-equilibrium phase transitions in a binary system of semiconductor elements is presented [12].

The absorption processes believed to be important for semiconductors are direct excitation of lattice vibrations with sub-band-gap, excitation of nearly free carriers by absorption of sub-band gap light, electron-hole excitation, and metallic behavior due to free carriers generated by laser light. Generally, melting and solidification are driven by heat and mass transport. The transport can occur by means of heat conduction and/or

diffusion in the liquid phase. A mathematical description of all relevant processes requires solving complex system of partial differential equations. In practice, this is difficult to do for phase-change problem. For this reason, simplified models are generally used that neglect less important factors and second order effects. The most popular approach is the thermal model for one-component system in one space dimensions, also known as Stefan's model.

G.D. Ivlev, and E.I. Gatskevich el (1998)[13] apply pyrometric measurements to obtain the epitaxial crystallization temperature of Si have been carried out for the (100), (110) and (111) crystallographic orientations of the laser irradiated surfaces of the samples. A ruby laser pulse duration was $10^{-7}$ s. Thermal radiation of melted Si was detected in green range of spectrum at the effective wavelength of 0.53 $\mu$m. The experimental data obtained have been analyzed on the basis of a nonequilibrium model of laser-induced liquid–crystal phase transitions. The orientation dependence of the epitaxial crystallization seems to be similar to that for the laser amorphization .

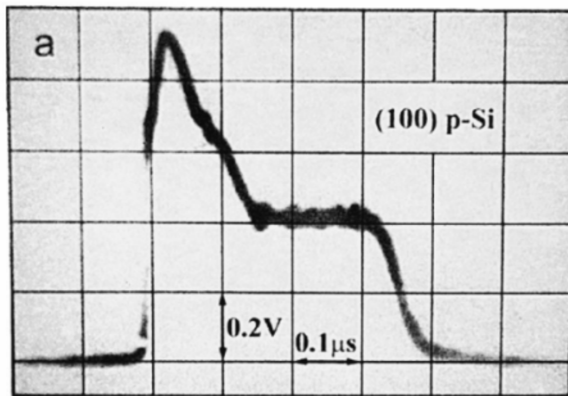


Figure 1-7 Temperature curve of the output signal of the pyrometer sensor.

John R. Ray and Mark D. Kluge et al (1989) [14] apply molecular-dynamics simulations to determine the steady-state velocity versus temperature relation for (001) solidification and melting of silicon using Stillinger-Weber potential to model the interaction between the silicon atoms. In their study, they show all the steady-state

velocity-versus-temperature values in Table 1.1

| Temperature (K) | Velocity (m/s) | Process |
|---|---|---|
| 950 | | no growth |
| 1000 | | partial growth of a few planes |
| 1050 | 10.23±1.48 | crystallization |
| 1250 | 16.43±1.04 | crystallization |
| 1350 | 19.40±2.01 | crystallization |
| 1450 | 14.32±0.70 | crystallization |
| 1550 | 11.95±0.69 | crystallization |
| 1600 | | no growth |
| 1700 | | no growth |
| 1750 | −21.22±1.04 | melting |
| 1850 | −22.20±0.80 | melting |
| 1950 | −43.00±1.92 | melting |
| 2050 | −54.86±2.14 | melting |

Table 1-2 Steady-state solidification (positive) and melting (negative) velocities as determined at each temperature using molecular-dynamics simulation.

According to John R. Ray and Mark D. Kluge et al study, we want to simplify th e grain growth model, and focus on only 1350K-1440K region. We assume grain growth only occurs in this region, and the latent heat influence the region, too. And in the following content, we ignore the nucleation effect and set the latent heat release regi on (1350K-1440K region), and set the maximum surface temperature 3000℃(like Figure 1-7).

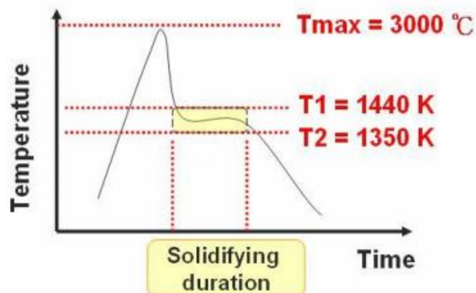


Figure 1-8 Temperature curve of a particular point versus the time

## 1.5. Motivation

In this thesis, we divide full content into four chapters. In chapter 1, the introduction for LTPS technology, ELA methods and position-control methods are mentioned introduced. In chapter 2, we discuss the model idea and set heat flux simulation parameters and the simulation results for the capping layer effects. In chapter 3, we discuss trench-assisted position control we did. Then, we find the optimized capping layer thickness (for $SiO_2$ and $SiN_x$), the optimized condition of trench and estimate the lateral grain growth size. In chapter 4, we would give a summary to the above results and talks about the future works.

# Chapter 2. Simulation

## 2.1. Heat Transfer Equation

Heat transfer is defined as the movement of energy due to a temperature difference. It is characterized by the following three mechanisms, Conduction, Convection, and Radiation. Considering three mechanisms, we assume all laser energy is transferred into samples, and neglect the heat loss due to convection and radiation.

The mathematical model for heat transfer by conduction is the heat equation:

$$\rho C \frac{\partial T}{\partial t} - \nabla \cdot (k \nabla T) = Q$$

Quickly review the variables and quantities in this equation：

T is the temperature.

$\rho$ is the density.

C is the heat capacity.

k is thermal conductivity.

Q is a heat source or a heat sink.

## 2.2. Heat flux Simulation

The software we use to simulate the laser crystallization process is FEMLAB which is a interactive environment for modeling and solving many kinds of scientific and engineering problems based on partial differential equations (PDEs). One of the tools is heat transfer simulation, and we choose the mode – transient analysis but not the steady state because we would try to analyzing the full process of the laser crystallization. We define the mesh shape to be triangle illustrated in figure 2.1, and the mesh density increasing would add our simulation time and the precision of the results simultaneously. We set each time step to be 1ns and the total simulation time to be 800ns such that we could confirm the accuracy and the completeness of the results at the same time. The following example will illustrate a simple simulation about the laser crystallization.

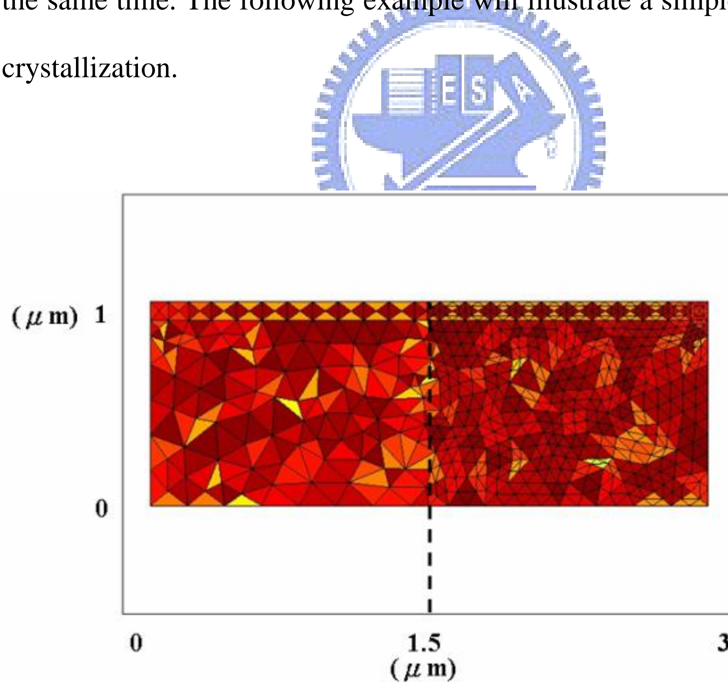


Figure 2-1 The left part of picture is the normal meshes in the structure and the right part is the refined meshes in the structure. The refine meshes would increase the ac curacy of the final result.

We assume a simple structure in Figure 2.2 and the dimensions of each side is labeled. The boundary conditions are then written as

$$\left.\frac{\partial T}{\partial x}\right|_{x=0} = 0, \qquad \left.\frac{\partial T}{\partial x}\right|_{x=4\mu m} = 0, \qquad \text{(Eq.2.1)}$$

$$\left.\frac{\partial T}{\partial y}\right|_{y=1.1\mu m} = 0 \qquad \left.T\right|_{y=0} = T_s = 23\ ℃ \qquad \text{(Eq.2.2)}$$

where T is the temperature and the $T_s$ is the ambient temperature and the initial sample temperature. The initial condition is $\left.T\right|_{t=0s} = T_s = 23\ ℃$ for all regions. An equation at time t is $\rho C \frac{\partial T}{\partial t} - \nabla \cdot (k \nabla T) = Q$ , where c and   are specific heat and thermal conductivity, respectively. Q is the heat generation or loss rate per unit volume. [15]

We have neglected the effects of infrared light emission and absorption, and therefore heat generation is only coursed by the absorption of the excimer laser light. The absorption coefficient,  , is a wavelength dependent value, and we measured it by n&k analyzer. It also a temperature-dependent value but its change is not essential. We used a fixed value of $7\times10^{7}\ m^{-1}$ for  . The part of the laser light irradiation is represented as the following equation:

$$aborption = T \times \alpha I_0(t, y)\exp(\alpha(y_0 - y)) \qquad \text{(Eq.2.3)}$$

where $y_0$ is the position at the top of the  -Si film ,$I_0$ is the light intensity irradiated to the sample surface and T is the transition coefficient. We have assumed that $I_0$ is a square-like time dependence that takes a constant value from t=0s to t=25ns. We also considered the additional heat stored and released in the silicon film during the crystallization process. We set a temperature regime from 1350 K to 1440K for the latent

heat stored in the silicon film at t<25ns (during laser irradiation) and released at t>25ns (after laser irradiation). The value of latent heat is 3000J/$cm^3$ and other parameters such as specific heat, thermal conductivity…etc. were list in Table 2.1.

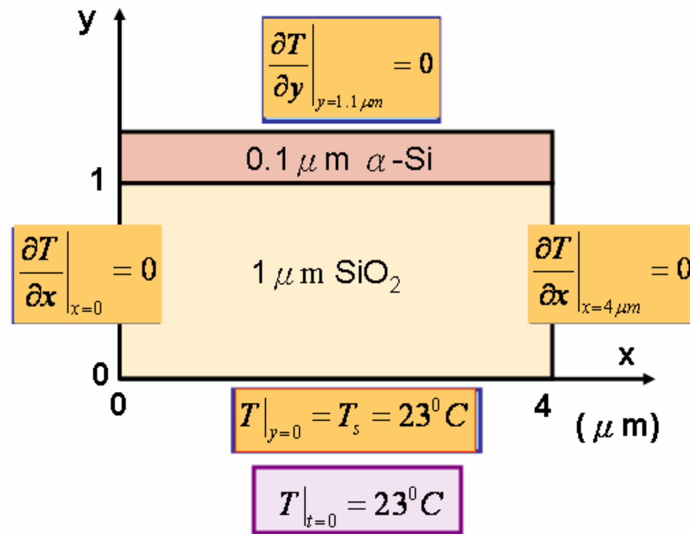


Figure 2-2 The structure for a simple simulation, the top layer is -Si and the bottom layer is $SiO_2$. The dimensions and the boundary conditions of each side are labeled on it.

| | a-Si | SiO2 | SiN |
|---|---|---|---|
| Absorption coefficient α ($m^{-1}$) | $7x10^7$ | 0 | $1.642x10^6$ |
| Latent heat L ($J/m^3$) | $3x10^9$ | N/A | N/A |
| Heat Capacity Cp ($J/m^3{*}k$) | 987.124 | 987.124 | 700 |
| Thermal Conductivity K (W/m*k) | 25 | 1.4 | 20 |
| Density ρ($Kg/m^3$) | 2330 | 2330 | 3100 |
| Cp($J/m^3{*}k$) x ρ($Kg/m^3$) | $2.3x10^6$ | $2.3x10^6$ | $2.17x10^6$ |
| Complex refractive index ( n+ iκ) | | | |
| n* | 3.226 | 1.506 | 2.265 |
| κ* | 1.897 | 0 | 0.0324 |
| N/A : Not Available, * : Measured by n&k analyzer | | | |

Table 2-1 Thermal conductivity, specific heat and other parameters used in the simulation. The value of absorption coefficient was measured by n&k analyzer.

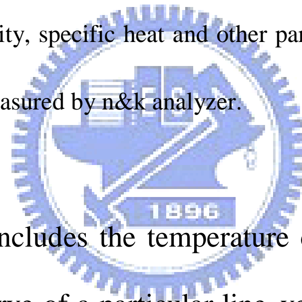

The simulation results includes the temperature curve of a particular point versus the time, the temperature curve of a particular line versus the time, the thermal distribution at a certain time, the contour lines of the temperature at a certain time and the heat flux at a certain time. The results we mentioned above will be illustrated in figure 2.3. From the temperature curve of a particular point versus the time we could understand the state of the silicon and from the contour lines of the temperature at a certain time and the heat flux at a certain time we could know the grain growth direction which is in the anti-direction of the heat flux. In 2.3 (b) there is no other special design, the laser energy tends to transfer to the substrate such that the grain would grow form the interface of two layers to the top surface vertically. In fi gure 2.3 (c) there exists a thermal platform region which represents the latent heat releasing during the liquid -phase Si transferring to solid-state Si. By analyzing figure 2.3(d) we could obtain a conclusion that after laser

irradiation (at 25ns) the most energy absorbed by the -Si layer. With the time passing, the exceeding heat transfer to the bottom $SiO_2$ layer and the temperature of the Si film tends to be same in each depth due to the high thermal conductivity of Si. Four results above are useful tools to analyze the crystallization process.

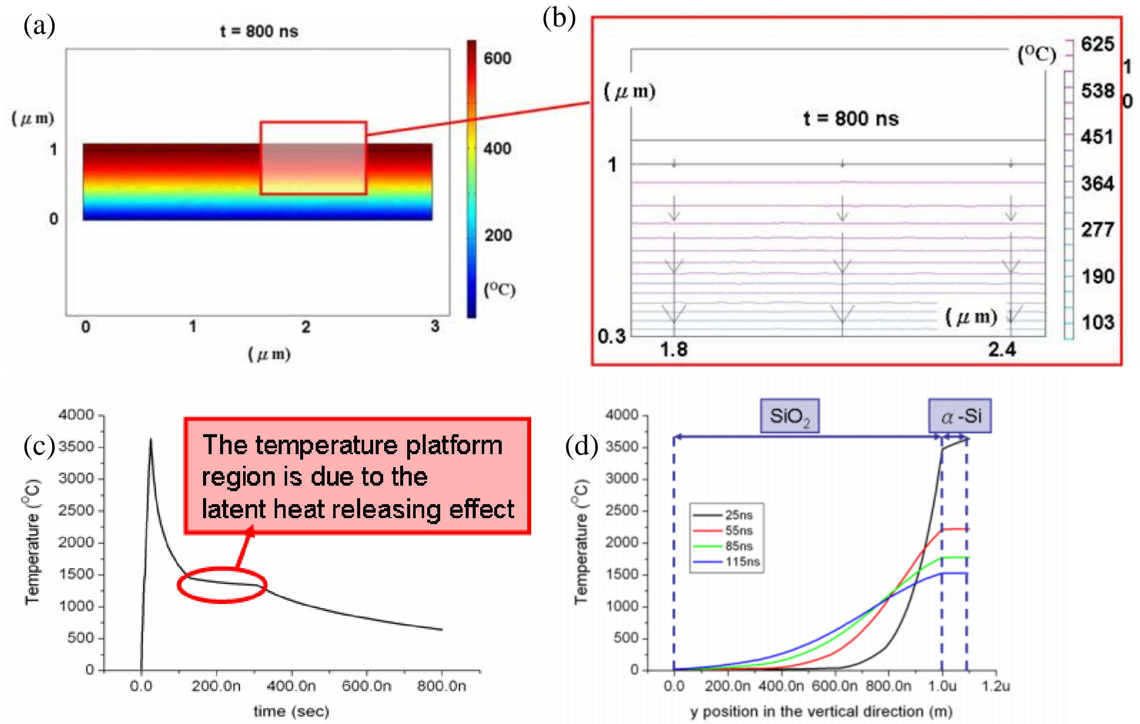


Figure 2-3 (a) Thermal distribution at a certain time = 800 ns, (b) the contour lines of the temperature and the heat flux at a certain time = 800ns (c) Temperature curve of a particular point (1.5μm, 1.1μm) versus the time (d) Temperature curve of a particular line (along the red line in figure 2.2) versus the time (at 25ns, 55ns, 85ns and 115ns)

Moreover, according to our simulation model, we can extract two parameters. First, we analysis the temperature-time plot (Figure 2-4 (a)) [13], and extract the latent heat releasing effect duration. The a-Si thin film undergoes phase transformation in this duration and the duration length determine the quality of the poly-Si thin film, so we define this duration as solidifying duration. In the following content, we will analysis

the grain growth quality by this value.

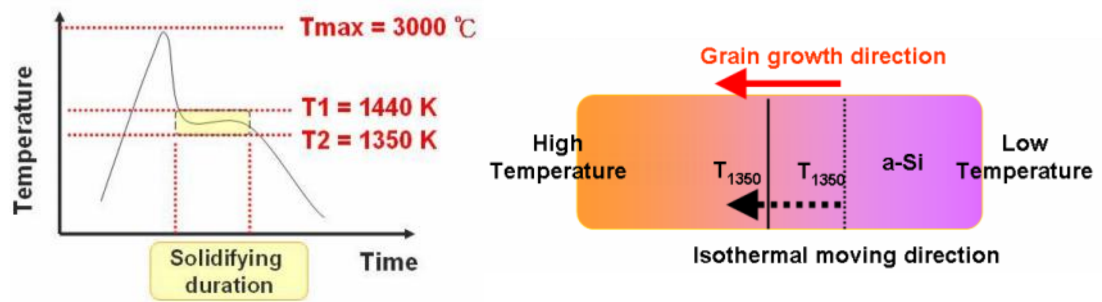


Figure 2-4 (a) Temperature curve of a particular point versus the time (b) isothermal movement diagram in solidifying duration.

And the other parameter is the solid-liquid interface velocity. In Figure 2-4, the interface velocity can be calculated by recording the movement of S-L interface. Because the super lateral grain growth has sequent moving isothermals perpendicular to the sample surface, we can estimate the velocity conveniently.

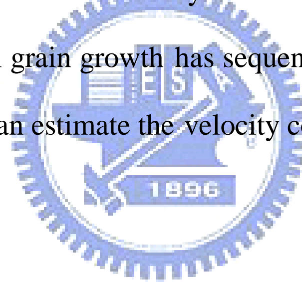

## 2.3. Simulation Condition with $SiO_2$ Capping Layer

Because the process window of conventional ELA is very small, capping layer on a-Si is usually used. We want to simulate this phenomenon and optimize the capping layer thickness.

Simulation condition：

The sample structure is like Figure2-5, a-Si(100nm)/$SiO_2$(1 $\mu$m), and vary the thickness of $SiO_2$ capping layer from 0, 100, 200, 300, 400nm.Then change the ambient temperature 300, 373, 473, 573, 673K, vary the thickness again.

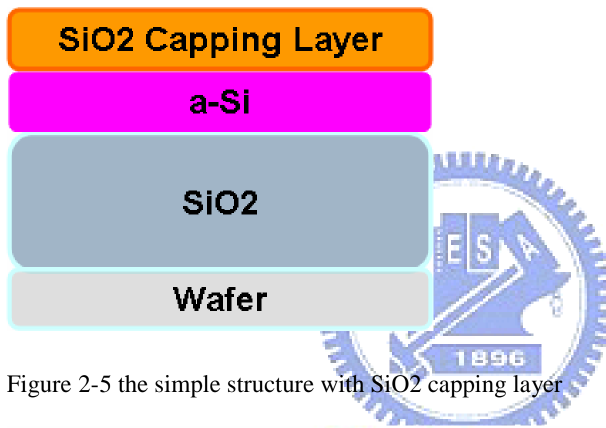


Figure 2-5 the simple structure with SiO2 capping layer

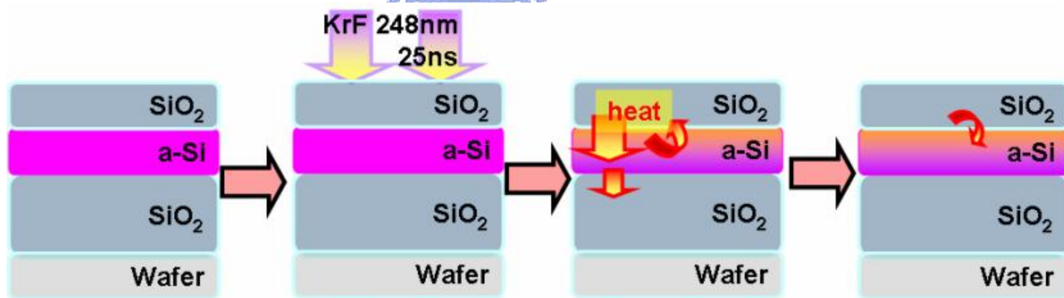


Figure 2-6 the process flow of heat transfer after laser irradiation with capping layer $SiO_2$

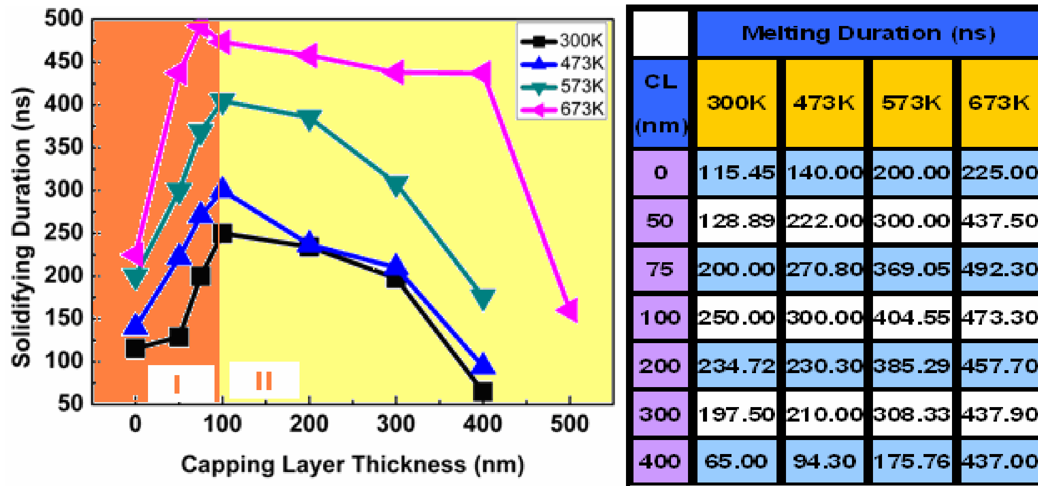


| CL (nm) | Melting Duration (ns) | | | |
|---|---|---|---|---|
| | 300K | 473K | 573K | 673K |
| 0 | 115.45 | 140.00 | 200.00 | 225.00 |
| 50 | 128.89 | 222.00 | 300.00 | 437.50 |
| 75 | 200.00 | 270.80 | 369.05 | 492.30 |
| 100 | 250.00 | 300.00 | 404.55 | 473.30 |
| 200 | 234.72 | 230.30 | 385.29 | 457.70 |
| 300 | 197.50 | 210.00 | 308.33 | 437.90 |
| 400 | 65.00 | 94.30 | 175.76 | 437.00 |

Figure 2-7 the solidifying duration diagram with different $SiO_2$ thickness and different ambient temperature

When KrF laser irradiates the sample (in Figure2 -6), only a-Si layer can absorb the laser energy, and then $SiO_2$ store the heat energy from the melted Si. Subsequently, the $SiO_2$ capping layer pass more heat energy to the solidifying sili con and prolongs the solidifying duration. There are two thermal effects ：heat reservoir effect, and heat sink effect. The heat reservoir effect means the capping layer can impermanent accumulate the heat from the melted a-Si layer and later feedback the heat to prolong the solidifying duration. On the contrary, the heat sink effect means the capping layer with lager heat capacity and thermal conductivity stores the heat from the melted a -Si and subsequently feedbacks less even no heat to the solidifying silicon, and results in sharp temperature decreasing.

In Figure2-7, when the thickness of SiO2 CL is smaller than 100nm, the solidifying duration increases with the thickness of CL, but dec reases quickly. And we find the optimized thickness, 100nm. As long as we raise the ambient temperature, the solidifying decreasing trend can be moderated. The region I is dominated by the heat reservoir effect, while the region II is dominated by heat sin k effect.

## 2.4. Simulation Condition with $SiN_x$ Capping Layer

We want to simulate this phenomenon and optimize the capping layer thickness.

Simulation condition：

The sample structure is like Figure2-6, a-Si(100nm)/$SiO_2$(1 μm), and vary the thickness of $SiN_x$ capping layer from 0, 100, 200, 300, 400nm.

Figure 2-8the simple structure with $SiN_x$ capping layer

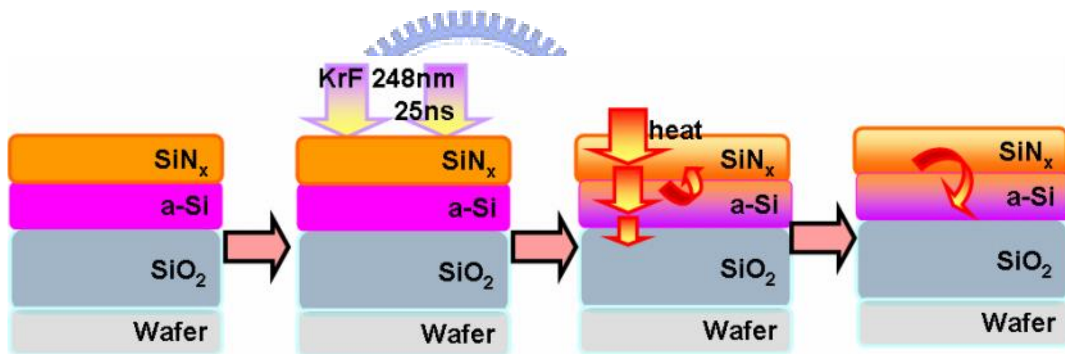


Figure 2-9 the process flow of heat transfer after laser irradiation with capping layer $SiN_x$

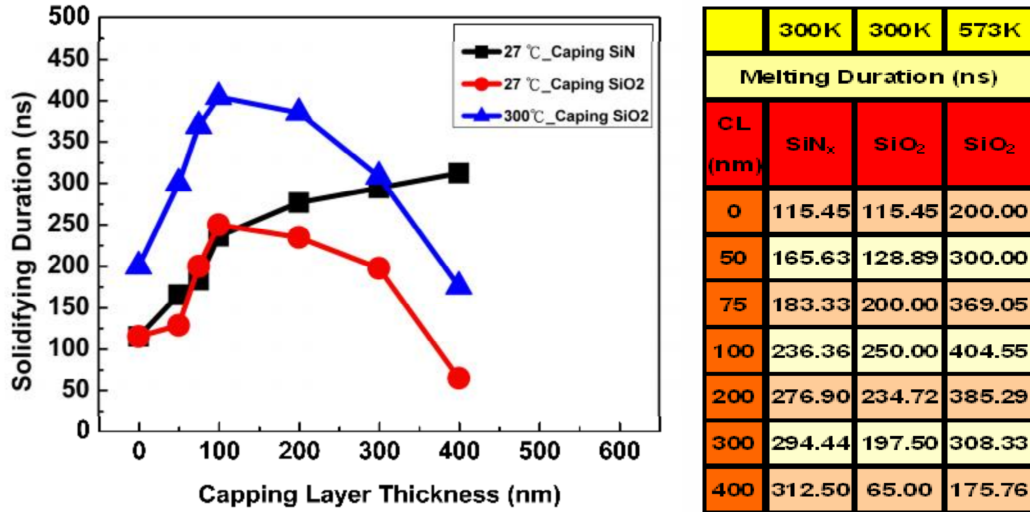


| | 300K | 300K | 573K |
|---|---|---|---|
| | Melting Duration (ns) | | |
| CL (nm) | $SiN_x$ | $SiO_2$ | $SiO_2$ |
| 0 | 115.45 | 115.45 | 200.00 |
| 50 | 165.63 | 128.89 | 300.00 |
| 75 | 183.33 | 200.00 | 369.05 |
| 100 | 236.36 | 250.00 | 404.55 |
| 200 | 276.90 | 234.72 | 385.29 |
| 300 | 294.44 | 197.50 | 308.33 |
| 400 | 312.50 | 65.00 | 175.76 |

Figure 2-10 the solidifying duration diagram with different $SiO_2$ thickness

In Figure2-10, the solidifying duration increases with the thickness of $SiN_x$ CL. When the thickness of $SiN_x$ is larger than 100nm the solidifying duration is still increasing. And it has potential to obtain comparable solidifying duration with capping $SiO_2$ layer with Ta=300℃ by increasing the thickness of $SiN_x$. In a word, capping $SiN_x$ can obtain higher solidifying duration at lower process temperature.

The heat capacity of $SiN_x$ (700 $J/m^3K$) is smaller than $SiO_2$ (987.124 $J/m^3K$), and the thermal conductivity of $SiN_x$ (20 J/mK) is larger than $SiO_2$ (1.4 J/mK). When the thickness of capping layer $SiO_2$ is lager than 100nm, the heat sink effect dominate the mechanism and the solidifying duration decrease with the thickness. Compared to the $SiO_2$, the heat sink effect should influence the SiNx capping layer seriously. However, the solidifying duration of $SiN_x$ is still increasing with the thickness over 100nm. There is some mechanism compete the heat sink effect. Comparing with the $SiO_2$ and $SiN_x$ parameters, we find the absorption coefficient of $SiN_x$ ($1.642 \times 10^6$ $m^{-1}$) is much larger than that of $SiO_2$ (0 $m^{-1}$). In a word, the $SiN_x$ can absorb KrF(248nm) laser energy but $SiO_2$ can't. When KrF laser irradiates the sample (in Figure2-9), the SiNx and a-Si can absorb the laser energy at the same time, and then SiNx store the heat energy from the

melted Si. Subsequently, the $SiN_x$ capping layer comparing with $SiO_2$ capping layer hands over more heat energy to the solidifying silicon and prolongs the solidifying duration. This phenomenon dominates the mechanism with the increasing thickness of $SiN_x$.

It is concluded that capping layer with higher absorption coefficient can decrease the heat sink effect and obtain longer solidifying duration. And $SiN_x$ capping layer with enough thickness can enhance more grain growth at lower process temperature.

# Chapter 3. Simulation with Trench-Assisted Position Control

Position control is an important technology for poly-Si TFT manufacturing. Now we want to simulate the trench-assisted position control method and optimize the condition, such as trench separation, trench depth, and thickness of $SiO_2$ CL.

## 3.1. Find out the Smallest Separation between the trenches and optimized trench depth

Find out the smallest separation between two trenches

Simulation Conditions：

We set each trench 300nm width and 300nm depth in a-Si(100nm) / $SiO_2$(1μm) structure (Figure3-1(a)), and vary the separation between trenches ：1μm, 2μm (Figure3-1(b)), and let the samples irradiated 250mj/cm2 laser intensity from the a-Si surface.

(a) (b)

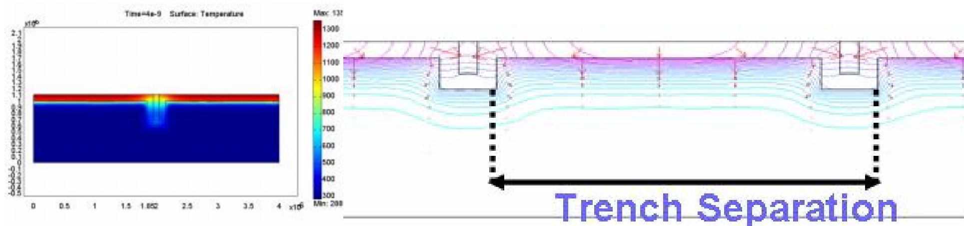


Figure 3-1 (a) Structure of each trench (b) The Structure of two trenches

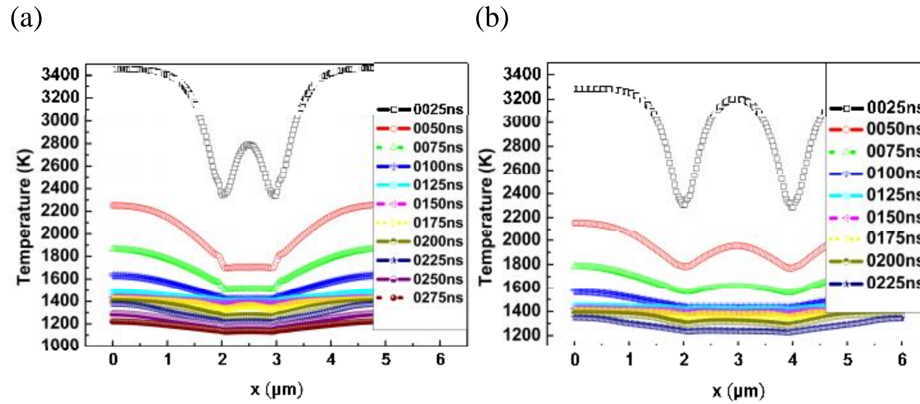


Figure 3-2 (a)Temperature curve on the a-Si surface with 1μm separation trench (b) Temperature curve on the a-Si surface with 2μm separation trench

In Figure 3-2 (a), we find that when the separation is 1μm, the temperature curve will not pull down so much that it seems has 1μm-width trench and create too many nuclei. And as long as the trench separation is larger than 2μm (Figure 3-2 (b)), the nearby trenches do not affect each other. And we assume there is only one nucleus in the trench that induces the lateral grain growth. In the following simulation, we all set the trench separation is 2μm.

Find out the optimized trench depth

Simulation Conditions：

We set each trench 100nm width in a-Si(100nm) / SiO2(1um) structure (Figure3-3), and vary the depth：200, 300, 400 nm with the laser energy density ：100, 150, 200, 250 mj/cm$^2$ (Figure3-1(b)). Finally, we can obtain the table 3-1.

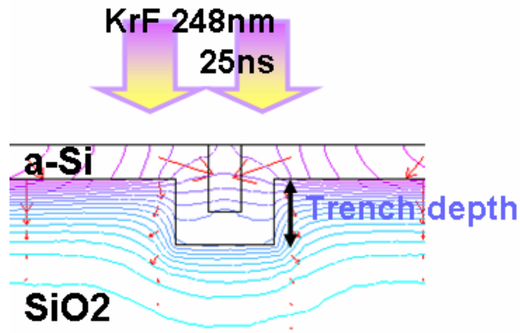


Figure 3-3 the structure for finding optimized trench depth

| Laer Energy Density / Trench depth | 100mj/cm2 | 150mj/cm2 | 200mj/cm2 | 250mj/cm2 |
|---|---|---|---|---|
| 200nm | 0ns | 55.71ns | 91.61ns | 135.5ns |
| 300nm | 0ns | 54.16ns | 110ns | 155ns |
| 400nm | 0ns | 14.44ns | 87.69ns | 153.9ns |

Table 3-1 the solidifying duration on the a-Si surface 2 $\mu$ m away from the trench with different trench depth and laser energy density.

In Table3-1, we find that the solidifying duration increasing with laser intensity. With considering let the a-Si surface temperature not over 3000℃, we choose the depth 300nm. And in the following simulation, we all set the trench depth 300nm.

## 3.2. Simulation Trench-Assisted Position Control with $SiO_2$ Capping Layer

As mentioned in 2.3, capping SiO2 layer can enhance the grain growth, in 3.2 we want to simulate the heat transfer in trench-assisted position control method and optimize the thickness of $SiO_2$ capping layer.

Set Simulation Conditions：

We set the trench depth 300nm in a-Si(100nm) / SiO2(1μm) structure (Figure3-4), and vary the thickness of SiO2 capping layer：0, 50, 75, 100, 200, 300, 400 nm and then, change the ambient temperature：300,673K. And we can obtain Figure 3-4.

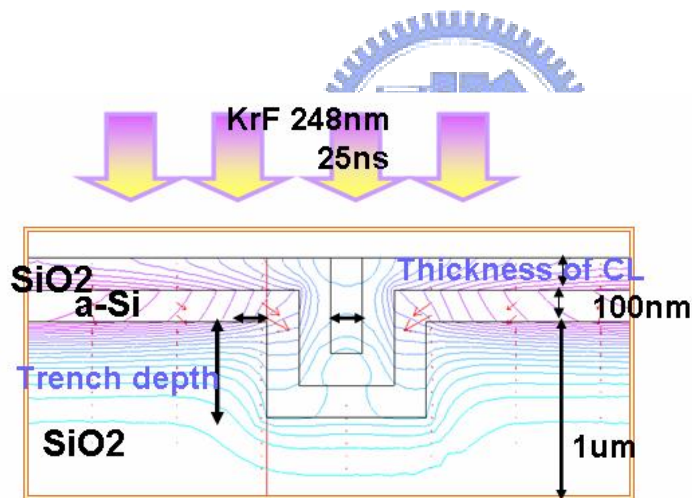


Figure 3-4the structure for finding optimized thickness of SiO2 CL

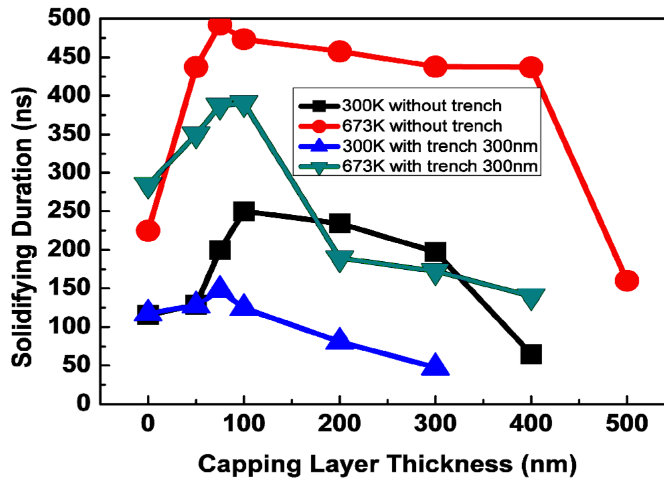


| | Melting Duration(ns) | | | |
|---|---|---|---|---|
| | With 300nm trench | | Without trench | |
| CLnm | 300K | 673K | 300K | 673K |
| 0 | 126.4 | 353 | 115.454 | 225.0 |
| 50 | 147.27 | 365.9 | 128.89 | 437.5 |
| 75 | 161 | 407.89 | 200 | 492.3 |
| 100 | 212.5 | 397.5 | 250 | 473.3 |
| 200 | 86.16 | 263.79 | 234.722 | 457.7 |
| 300 | 76 | 225 | 197.5 | 437.9 |
| 400 | 55.97 | 132.5 | 65 | 437.0 |

Figure 3-5 the solidifying duration diagram with different $SiO_2$ thickness

In Figure3-5, we can find that adding trench will lower the solidifying duration intensely and increasing the ambient temperature also can increase the solidifying duration. With and without trench both have optimized thickness of $SiO_2$ capping layer, about 100nm. When the thickness of SiO2 capping layer is over 100nm, the heat sink effect dominates the mechanism seriously.

## 3.3. Calculation of Solid-Liquid interface and Estimation of Grain Size

By recording the 1350K isothermal movement (Figure 3-6), we can calculate the isothermal velocity, namely S-L interface velocity. We analyze 1350K-isothermal movement with different thickness at the ambient temperature 27℃, and obtain Figure3-6. In Figure3-6, when the thickness of $SiO_2$ capping layer smaller than 200nm, the solidifying duration decrease with the $SiO_2$capping layer thickness. The heat reservoir effect dominates the mechanism and slow the1350-isothermal. Otherwise, when the thickness of $SiO_2$ capping layer larger than 200nm, the solidifying duration increase with the $SiO_2$capping layer thickness. The heat sink effect dominates the mechanism and speed the1350-isothermal. The velocity ranges from 0.015~0.020 (μm/ns). It is proven (In Figure3-9, the real simulation result) that trench-assisted position control method indeed induces lateral grain growth.

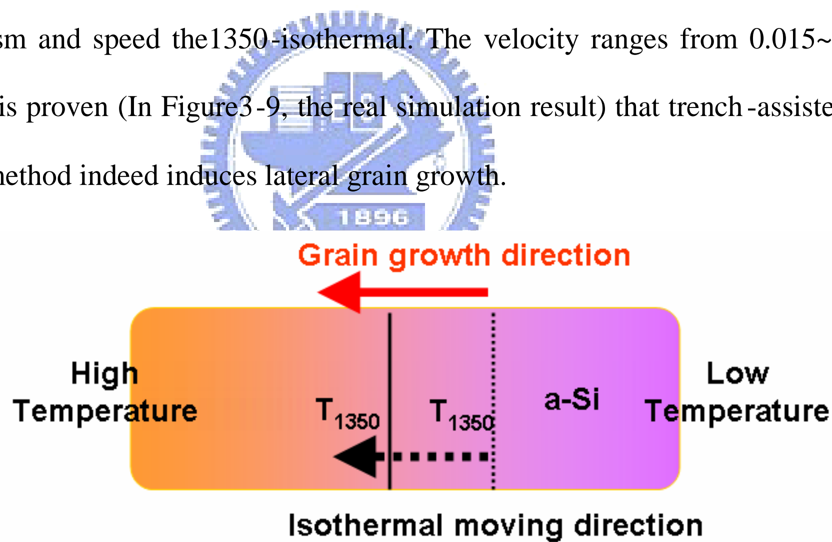


Figure 3-6 the isothermal movement diagram in solidifying duration.

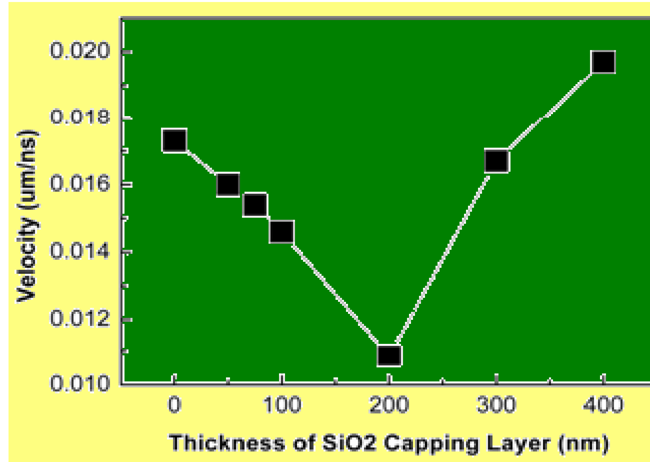


Figure 3-7 S-L interface velocity diagram at ambient temperature 27℃ with different thickness of $SiO_2$ capping layer.

(a)

(b)

(c)

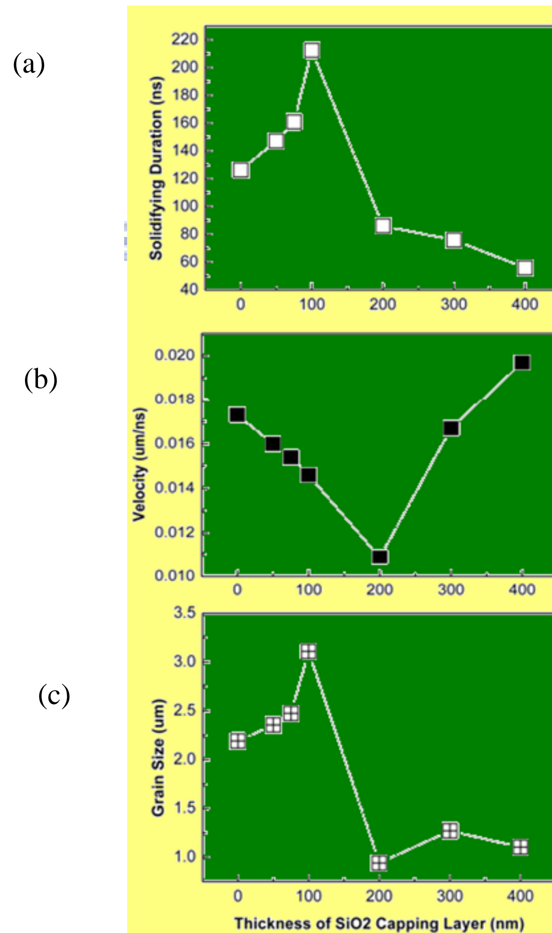


Figure 3-8 (a) Solidifying duration diagram, (b) S-L interface velocity diagram and (c) the estimation grain size diagram at ambient temperature 27℃

We multiply the solidifying duration and the S-L interface velocity to get the grain size estimation diagram. Comparing with the three plots, Figure3-7 (a) Solidifying duration diagram, (b) S-L interface velocity diagram and (c) the estimation grain size diagram at ambient temperature 27℃ , we can obtain optimized the thickness of $SiO_2$ capping layer and the estimation of the grain size, 3um, induced by the trench to one side. In a word, we can obtain maximum grain size, 6um.

Besides, the heat sink effect dominates the Solidifying duration diagram and S-L interface velocity diagram at different thickness of $SiO_2$ capping layer, 100nm and 200nm. However, the solidifying duration is a strong key parameter, so the optimized grain size is at 100nm-thickness.

Figure 3-9 1350-isothermal movement at Ta=27℃ with trench 300nm depth and no capping layer

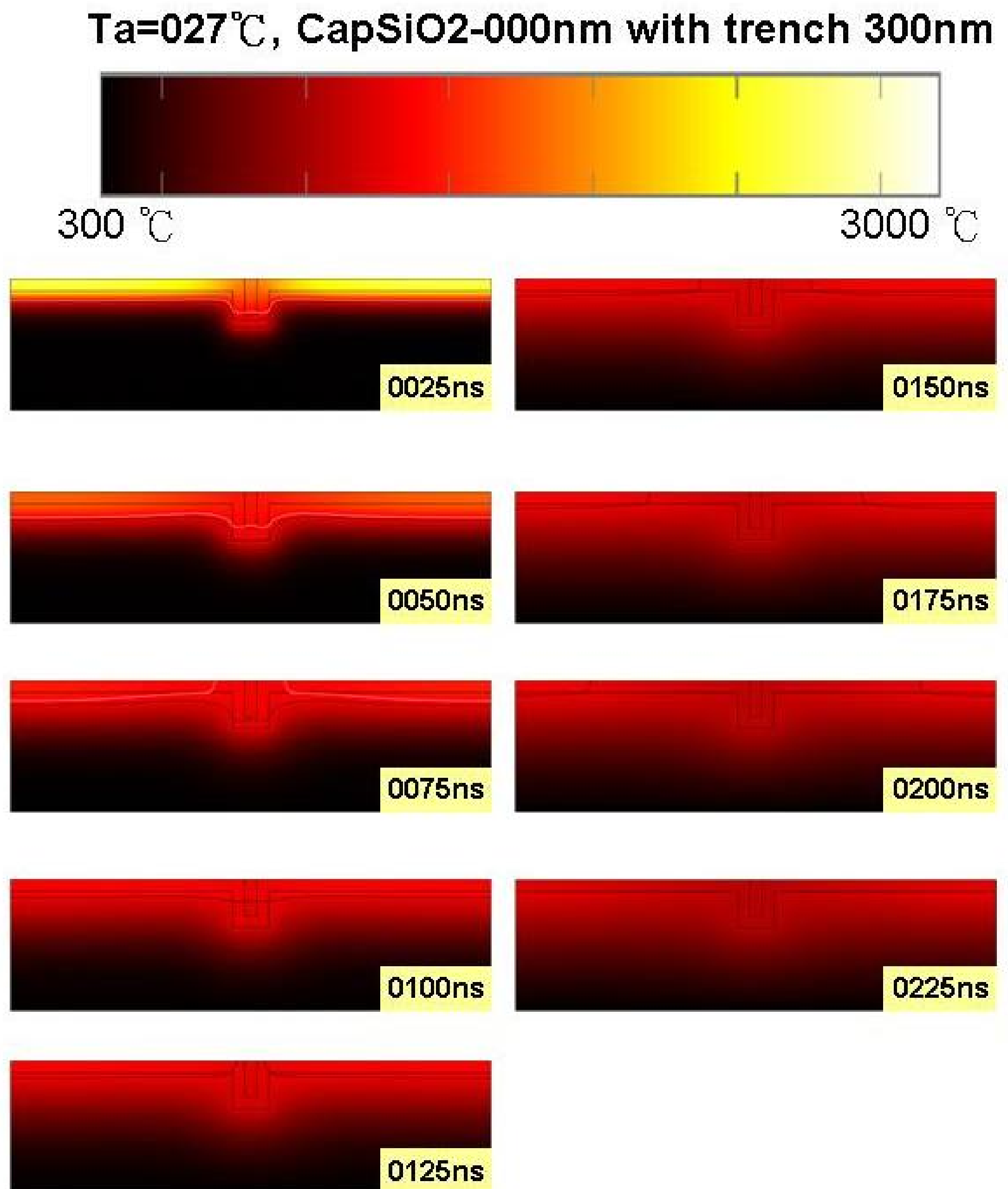

# Chapter 4. Summary and Future Work

## 4.1. Summary

In this thesis we simulate the heat transfer inside the a-Si thin film. And by defining latent heat process region, the temperature distribution among the samples can be successfully measured.

In the following, in order to prolong the solidifying duration, the heat-retaining layer is utilized, such as SiO2 and SiN materials. By measuring the n&k of the capping layer, the absorption($\alpha$) and transmittance($T$) are concerned in the simulation. And we find that the thickness of $SiO_2$ capping layer has an optimized value 100nm with and without trench, and that of SiNx capping layer thicker than 100nm has better performance on solidifying duration compared with the same thickness of $SiO_2$ capping layer.

Moreover, we simulated the trench-assisted ELA. And we find out its optimized trench depth, 300nm, and its smallest separation, 2$\mu$m. It is proved that trench-assisted ELA can induce lateral grain growth by observing the isothermal diagram. By recording the movement of the 1350K isothermals, we can calculate the isothermal moving velocity, namely solid-liquid interface velocity. Finally, we can estimate the grain size from a trench to one side is about 3$\mu$m for an optimized condition. In a word, utilizing a trench can induce about 6$\mu$m lateral grain growth.

## 4.2. Future Work

First, we may involve the temperature dependent Cp(T) and K(T) in our simulation to describe the latent heat closely to heat transfer in the model.

Second, we can simulate the heat transfer in other device structure.

Finally, we can testify and optimize other capping materials on a-Si as long as we have enough parameters.

# Reference

[1] P. K. Weimer, "**The TFT -- a new thin film transistor**," Electron Devices, IRE Transaction, p. 421, 1961.

[2] T. P. Brody, J. A. Asars, and G. D. Dixon, "**A 6 x 6 inch 20 lines-per-inch liquid crystal display panel**," Electron Devices, IEEE Transactions, vol. 20, p. 995, 1973.

[3] P. G. LeComber, W. E. Spear, and A. Ghaith, "**Amorphous-silicon field-effect devices and possible applications**," Electron. Letter, vol. 15, p. 179, 1979.

[4] G. Harbeke, L. Krausbauer, E. F. Steigmeier, A. E. Widmer, H. Kappert, and G. Neugelbauer, "**High quality polysilicon by amorphous low pressure chemical vapor deposition**," Applied Physics Letters, vol. 42, p. 249, 1983.

[5] A.T. Voutsas, M.K. Hatalis, "**Structure of As-Deposited LPCVD Silicon Films at Low Deposition Temperatures and Pressures**." J. Electrochem, Soc. 139 (1992) 2659.

[6] A.T. Voutsas, M.K. Hatalis, "**Deposition and Crystallization of A-Si Low Pressure Chemically Vapor Deposited Films Obtained by Low Temperature Pyrolysis of disilane**," J. Electrochem, Soc. 140 (1993) 871.

[7] A.T. Voutsas, M.K. Hatalis, "**Structural characteristics of As-deposited and Crystallized Mixed-Phase Silicon Films**," J. Electrochem, Soc. 23 (1994) 319.

[8] H. Kuriyama, S. Kiyama, S. Noguchi, T. Kuwahara, S. Ishida, T. Nohda, K. Sano,H. Iwata, H. Kawata, M. Osumi, S. Tsuda, S. Nakano and Y. Kuw ano, "**Enlargement of poly-Si film grain size by excimer laser annealing and its application to high-performance poly-Si thin film transistor**," Jap. J. Appl. Phys., vol. 30 (12B), p.3700, 1991.

[9] Mitsuharu Tai, Mutsuko Hatano, Shinya Yamaguchi, Takeshi Noda, Seong-Kee Park, Takeo Shiba, Member, IEEE,and Makoto Ohkura, Member, IEEE ,

"**Performance of Poly-Si TFTs Fabricated by SELAX** ," IEEE TRANSACTIONS ON ELECTRON DEVICES, VOL. 51, NO. 6, JUNE 2004

[10] Masakiyo Matsumura, Chang-Ho Oh, "**Advanced excimer-laser annealing process for quasi single-crystal silicon thin-film devices** ," Thin Solid Films 337 (1999) 123-128

[11] R. Cerny, V. Vydra , P. Prikryl , I. Ulrych , j. Kocka c, K.M.A. E1-Kader ,Z. Chvoj , V. Chfib, "**Theoretical and experimental studies of a-Si:H recrystallization by XeC1 excimer laser irradiation**," Applied Surface Science 86 (1995) 359-363.

[12] R. Cerny, P. Prˇikryl, "**Non-equilibrium model of laser-induced phase change processes in amorphous silicon thin films**," Physical Review B, Vol57, 1, 1998.

[13] G.D. Ivlev, E.I. Gatskevich, "**Solidification temperature of silicon surface layer melted by pulsed laser irradiation**," Applied Surface Science 143, 265–271, 1999.

[14] John R. Ray, Mark D. Kluge , "**Velocity versus temperature relation for solidification and melting of Si A molecular-dynamics study** ," Physics Review B, Vol 39, No3, 1989.

[15] Wen-Chang Yeh, and Masakiyo Matsumura "**Numerical Calculation of Excimer-Laser-Induced Lateral-Crystallization of Silicon Thin-Films**," JJAP, Vol 40, pp492-499, 2001.